Balancing Long-Term Plasticity Mechanisms at the Purkinje Cell in the Olivocerebellar System

Master Thesis

T. Hoedemakers - 4950593

Balancing Long-Term Plasticity Mechanisms at the Purkinje Cell in the Olivocerebellar System

Master Thesis

by

T. Hoedemakers

in partial fulfillment of the requirements for the degree of

Master of Science
in Biomechanical Design

at the Delft University of Technology

Student Number: 4950593

Supervisors:	prof. dr. ir. D. A. Abbink,	TU Delft
	dr. ir. M. Negrello,	TU Delft & Erasmus MC
	dr. ir. L. Peternel,	TU Delft
Thesis committee:	prof. dr. ir. D. A. Abbink,	TU Delft
	dr. ir. M. Negrello,	TU Delft & Erasmus MC
	dr. ir. L. Peternel,	TU Delft
	dr. M. Jafarian,	TU Delft

Cover picture : `http://www.robotspacebrain.com/art-inspired-by-neuroscience-2/`.

TU Delft

Preface

This master thesis is carried out in partial fulfillment of the requirements for the degree of Master of Science in Biomechanical Design at the Delft University of Technology. In this thesis, a phenomenological model of the olivocerebellar system with balancing of long-term potentiation and long-term depression was developed.

My thanks and gratitude go to Dr. Ir. Luka Peternel and Dr. Ir. Mario Negrello who provided supervision during the project. Also, I would like to thank my parents for their unconditional support, even though they did not understand a single word of what I was doing.

T. Hoedemakers
Delft, October 7, 2020

Balancing Long-Term Plasticity Mechanisms at the Purkinje Cell in the Olivocerebellar System

Thijs Hoedemakers
Supervised by: Luka Peternel (TU Delft) and Mario Negrello (TU Delft & ErasmusMC)

ABSTRACT

The olivocerebellar system plays a crucial role in control of movements of the human body in terms of coordination, precision and timing. Long-term plasticity is directly linked to motor learning and control. In this research, we developed a phenomenological model of the olivocerebellar system with balancing of long-term potentiation (LTP) and long-term depression (LTD) at the parallel fiber-Purkinje cell (PF-PC) synapse. By ranging the PF input over frequencies, we found that PCs can select frequencies in a highly non-linear manner. There is a sharp contrast in synaptic weight change between neighbouring frequencies, which is caused by the temporal spiking property of the inferior olive (IO) cell. This research found a novel signal processing capability of the PC.

Index terms **- Olivocerebellar System, Long-term plasticity, Resonance, Homeostasis, Purkinje Cell, Inferior Olive**

I. INTRODUCTION

The control of the human body is inherently complex when you consider, for a start, the degrees of freedom, the amount of redundant actuators, and the ability to adapt to new situations. There is currently no man-made control structure, which controls the body the way the brain does. Therefore, studying the neural mechanisms of human motor control can therefore significantly contribute to the development of robotic systems.

In the control of the human body, the cerebellum plays a fundamental role. Cerebellar lesions are characterized by ataxic motor syndromes, which affect speech [1], ocular motor control and learning [2], [3], and stability of gait [4]. In all ataxic motor syndromes there is an ongoing mismatch between the inputs and the response to these inputs. The inputs to the system, coming from both the spinal cord and the cerebrum, suggest that the role of the cerebellar system cannot be separated from either sensory or motor functions [5]. The cerebellum plays a role in both motor learning and motor control [6], however the way it performs its functions remains unknown. We may take speculative stance and create a model that captures known physiological, anatomical and dynamical features of the cerebellar system. Subsequently, use reverse-engineering to explain the emergent properties. A link has to be created between brain mechanisms and psychological functions. A phenomenological model of the cerebellar system (i.e. a model that is consistent with known facts of the cerebellar system, although not derived from first principles) can provide insights on the processes that drive its function.

We developed a phenomenological model that uses an unsupervised learning method, to uncover the methods used by the cerebellar system. Since we do not prescribe an explicit learning method to the system, the system is said to adapt, and consequently learn, in an unsupervised manner. By applying this method, one does not assume a certain function of the system itself, but the observations can be used to verify or validate hypotheses. The method is in contrast to Marr-Albus-Ito type models [7], which assumes the method of learning. We think there is more to discover and therefore use an unsupervised, physiological method that explores the processes that drive learning. This brings us closer to an understanding of the underlying mechanisms occurring in the cerebellum, which an organism on a higher-level uses to attain a certain function. This method is applied in this thesis to analyze the function and dynamics of the cerebellar system, with a primary focus on the long-term plasticity mechanisms.

The activity-dependent adaptation of synaptic weights ('plasticity') is thought to be directly linked to learning. Examples being, simple and complex multi-joint movements in monkeys [8], adaptation in eye movements (vestibulo-ocular reflex (VOR) [9]), and classical eye-blink conditioning [10]. Even though there is plasticity at all the synapses of the cerebellar cortex [11], the most researched and associated with cerebellar learning is the plasticity at the Purkinje cell (PC) [12], [13]. Therefore, the focus in this research of plasticity is at the PC and balancing of the two long-term plasticity mechanisms that are thought to drive learning. Long-term plasticity is defined as a synaptic weight change that is maintained for prolonged periods of time (minutes to hours).

The two distinct types of long-term plasticity mechanisms at the PC, that can adapt the synaptic weight and therefore enhance learning, are long-term potentiation (LTP) and long-term depression (LTD). Which plasticity is at play, partly depends on the type of spiking of the PC. PCs can produce both simple spikes (SS), with a frequency around 100 Hz, and complex spikes (CS), with a frequency around 1 Hz. SS can occur either

spontaneously or driven by parallel fibers (PF), whereas CS originate solely from the inferior olive cell (IO). A single PC receives input from a single IO cell [14], [15] but its connection, with approximately 1500 release sites, is extremely powerful [16]. The parallel fiber inputs are, with ~200.000 contacts, the most abundant synaptic connection in the vertebrate central nervous system [17]. Whether the PF-PC synapse depresses or potentiates is dependent on the presynaptic activity. LTP, in general, states that when the presynaptic neurons fires often, the postsynaptic neurons starts increasing the density of α-amino-3-hydroxy-5-methyl-4-isoxazolepropionic acid (AMPA) receptors in the dendrite. The presynaptic activity for LTP is solely coming from the PF connection and the postsynaptic cell is the PC. On the other hand, when the IO triggers a CS in the PC, the simultaneously active PF undergo LTD. The PF-PC synaptic strength can move in both directions. The CF can be regarded as a polarity switch between LTP and LTD [18].

The IO and the CSs it triggers in the PC are therefore of major importance in determining the synaptic weights. Simultaneous electrode recordings of a group of PCs have shown that CS occur synchronously among the group [19], [20]. This suggests that there are groups of IO cells that fire rhythmically. Electronically coupling via gap junctions of the IO cells is thought to be the mechanism underlying the synchrony of the CS [21]. These gap junctions are mainly located at the dendritic spines and are required to cluster oscillatory behavior of the IO. While most IO cells are intrinsically oscillatory, i.e. they show subthreshold oscillations (1-10 Hz with an amplitude of 1-20 mV), large sustained oscillations only occur in a network which allows intercellular flow [22], [23]. These dynamical, oscillatory properties of the IO cell are of major influence on the response of the system. It can guide or show certain resonances of the olivocerebellar loop due to its reverberating nature. The details of the coupling is included in our model.
The activity from the IO cell can reverberate back onto the IO cell, due to the connectivity of the olivocerebellar system. When a spike of an IO cell produces a CS in the PC there is often a pause in the SS activity following this event [24]. Consequently, the deep cerebellar nuclei (DCN) receive less inhibition and produce a short burst of rebound spikes after a delay of around 100 ms [25]. This delay is congruent with the supposed interspike interval of the population of the IO cells. The rebound activity of the DCN is directly projected onto the IO cell [26], which closes the olivocerebellar loop and raises the question what the resonant properties of the system are. These properties can yield selection of certain PF inputs. This is concluded by observing the response of the loop to a range of single frequency inputs. It was found that the loop selects certain frequencies with the implemented plasticity mechanism, i.e. potentiation of the PF-PC synapse. There are different models on synaptic modification, which are evaluated on their capacity to capture the biological properties of the plasticity at the PF-PC synapse.

The earliest models of synaptic change are based on neuronal activity at the different synapses [32], [33]. These models follow the Hebbian rule which states: when neuron A connects to neuron B and it fires repeatedly and persistently, some growth process or metabolic change takes place [34]. Due to this change, both cells change such that neuron A's efficiency increases as well as the firing rate of neuron B increases. This learning rule implies a growth without bound and does not yield selectivity for different input patterns, which is experimentally observed in neurons. Hebbian learning assumes the presence of backpropagation of postsynaptic spikes, which was later found to be present in most neurons [29]. A visualization is presented in Figure 1(b). Cooper, Liberman, Oja (CLO) theory [30] combines *anti-Hebbian* learning, which adds a component that depresses when the postsynaptic neuron firing rate is below a certain threshold, with Hebbian learning, as depicted in Figure 1(c). This process confers selectivity, since neurons only respond to certain inputs after learning.
However, CLO is unstable since the value for the threshold θ_m can either be too large, which results in depression and all weights weaken to zero, or it can be too small, which makes every weight rise indefinitely. By making θ_m adjustable to the average firing rate of the postsynaptic

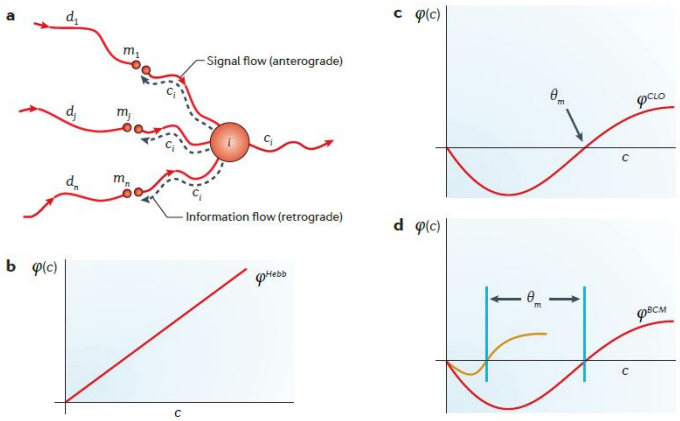

Fig. 1. Theories of synaptic modification [27], [28]. (a) cell i is the postsynaptic cell and receives signal flow (anterograde) translated from the firing rates of the presynaptic cells d_i, d_j and d_n at the synapses m_i, m_j and m_n. The information flow (retrograde, dotted line) is the information on the firing rate of the postsynaptic cell i. In most neurons back propagation is ensured by Na^+ channels in the axon, soma and dendrite [29]. (b-d) These three figures show theories of synaptic modification. $\phi(c)$ is the function that determines the amount of integrated response (c) of the postsynaptic neuron. (b) The Hebbian learning rule. The response increases monotonically with the integrated postsynaptic response. (c) The CLO learning rule combines the Hebbian learning rule with an *anti-Hebbian* rule to ensure selective responses [30]. When the input evokes a postsynaptic response which is higher than the threshold value θ_m, the synaptic connection potentiates and when it is lower, it depresses. The amount of difference with the threshold determines the level of depression/potentiation. (d) The BCM theory [31], makes θ_m adjustable to the average firing rate of the postsynaptic neuron. There are two different cases presented.

neuron homeostasis is guaranteed. This is embodied by the Bienenstock, Cooper, Munro (BCM) theory, as shown in Figure 1(d). BCM requires bidirectional synaptic modification, as is the case for long-term plasticity mechanisms, described above. The synaptic weights move towards a stable value where they only respond to certain part of the input pattern, meaning there is stimulus selectivity [27].

The plasticity at the site of the PC cannot be captured by the BCM theory due to the many complexities. Both, the input coming from the CF, and the PF have excitatory connections to the PC and therefore do not directly depress the neuron. The PC has to balance both LTP and LTD which operate at different frequencies, ~100 and ~1 Hz accordingly. The effect of the CF can only lead to LTD if accompanied by PF activity. Furthermore, it does not account for the limited receptor density present in the dendrite of the PC. Modelling plasticity is only one aspect in the context of cerebellar modelling. The state-of-the-art on cerebellar modelling can give insight in their methods, strengths, and weaknesses.

Modelling of the cerebellar system can be done on different levels and with diverse goals in mind. Our goal is to find emerging neural mechanisms of the cerebellar system in the context of learning. We examine three state-of-the-art approaches that were designed to pursue different specific research goals, and evaluate their ability to contribute to our research goal.
Firstly, a physiological state-of-the-art cerebellar model was created by Geminiani et al [35]. The model is able to capture experimentally observed phenomena (burst-pause in PC, pause-burst in DCN) and has the most complete cellular representation. However, there is no plasticity rule implemented and it has no functionality in context of learning.
Secondly, on a functional level, the cerebellar model of Casellato et al. [36] can learn to perform different sensorimotor tasks in real-time with on the fly adaptation. A caveat of this model, is that the role of the IO cell is reduced to the provider of an instruction signal for learning. The model therefore learns in a supervised manner, which provides no explanation of the underlying mechanism used by the cerebellum. Also, as mentioned before, the IO comprises of much more complexity. The role of the IO cell as provider of error signal is debatable, as it is shown that groups of IO cells show spontaneous quasiperiodic rhythmic activity [37], [38]. The CSs are not only driven by inputs or error and are therefore unlikely to exclusively encode error.
Finally, a method used by infants to get familiar with their own sensor-motor relationships is called motor babbling. The state-of-the-art, cerebellum-inspired, unsupervised learning method is shown in [39]. The method is able to control the motion of a redundant plant. Nonetheless, there is little regard for anatomical accuracy. And Hebbian learning is used, which, as shown before, is unstable.

Resulting from these state-of-the-art models, our model satisfies the following prerequisites:

- *p1* : Functionality in context of learning
- *p2* : Unsupervised adaptation
- *p3* : Physiological accuracy

In line with the aforementioned modelling approach, we developed a novel plasticity mechanism, that is able to overcome the above-mentioned problems of modelling the plasticity at the level of the PC. The model aims to describe the empirical relation between the PF-PC plasticity and the PF input, in context of the cerebellar loop. The biological observations drive the requirements of the entire model and the plasticity mechanism. We model the dynamical properties of the IO in detail due to its considerable influence on the loop dynamics. The emergent properties of the olivocerebellar loop are analyzed with different PF input frequencies.

Our plasticity mechanism can account for the difficulties that present themselves at the PC. The biological constraints that drive the plasticity mechanism can satisfy the following requirements:

- *r1* : Account for the inconsistent firing rate of PCs and IO cells
- *r2* : Final weights, after adaptation, settle on different values for different PCs
- *r3* : Weight change only occurs if there is causal relation between presynaptic activity and change in firing frequency
- *r4* : The weights do not grow without bounds
- *r5* : Ensured homeostasis at the synapse and on a network level

Once our model and plasticity mechanism obeys the biological criteria, the weight changes are analyzed for a range of PF input frequencies. A novel signal processing capability of the PC was found.

II. Method

A. Introduction to the model

The model that is used to reverse-engineer properties of the cerebellar system consists of three types of cells: Purkinje cells (PC), deep-cerebellar nuclei (DCN) and inferior olive cells (IO). The network consists of 10 PCs, 20 DCN, and 20 IO cells. The size of the network represents a cerebellar module. A cerebellar module is defined here, as a parasagittally arranged zone of PCs, their projection to a well-defined region of DCN, and the IO cells of a distinct region which synapse onto PCs [40]. An other reason for the network size is that, while it can represent the dynamical loop properties, it remains computational tractable.

The DCN and PC neurons are adaptive exponential leaky integrate-and-fire (aEIF) neurons [41]. The parameters of the cells are based on neural and physiological data to

match the firing frequencies observed in experiments [42]–[44]. The differential equation that is used to describe the membrane potential is given by

$$\frac{dV}{dt} = \frac{1}{C_m}(f(V) - w + I), \tag{1}$$

in which C_m is the membrane capacitance, $f(V)$ is a function that captures the passive properties of the cell and the spiking mechanism, w is an variable that captures the adaptation current, and I is the synaptic current. Further elaboration of the equations and parameter values can be found in Appendix A.

The model of the IO cell is a two-compartment model of the soma and the dendrite. It is a modification of the Schweighofer model [45]. The model is able to produce spiking and oscillatory behavior. An additional property of the IO cell model is the possible presence of gap junctions between the IO cells. As discussed in Sec I, the gap junctions facilitate the presence of large and sustained subthreshold oscillations. By having the ability to electronically couple the IO cells, the effect of this connection can be observed. The electronic coupling is represented as a current flowing between the dendrites of the cells. The implementation and details of the IO model can be found in Appendix A.

B. Prerequisites of the model

As discussed in Sec I, there are three prerequisites that are taken into account, that follow from the state-of-the-art approaches of cerebellar modelling. Prerequisite *p3 Physiological accuracy* is elaborated in Table I, and the method of validation is presented.

The connectivity between the different cells are presented in Table II and based on anatomical observations. The amount and shape of the PF inputs to the cerebellar system is under control of the user of the model. In this research the PF input is kept at two with a sinusoidal shape. In Table II, the static component of the weight is presented, while during plasticity these weights change over time.

TABLE II
SYNAPTIC CONNECTIVITY BETWEEN THE DIFFERENT NEURONS

Synapse (Source-Target)	Connectivity	Static Weight
PF - PC	2 - 1	0.5
PC - DCN	1 - 10	1
IO - PC	1 - 1	1
DCN - IO	1 - 10	1

C. Plasticity Mechanism

The two plasticity mechanisms at play, that determine the change of synaptic strength of PF-PC synapse, are LTP and LTD. The PC is able to balance these two mechanisms. Since the mechanisms are purely biologically inspired and implemented without a prior function or error-driven functionality, prerequisite *p2 Unsupervised adaptation* is met. In this section, both the equations that describe its behavior, and the assumptions are presented for the implementation of the plasticity mechanism.

It is assumed that all PCs receive same amount of input current from postsynaptic activity. Since the model is evaluated with at its maximum two input, the initial weights are set equal to 0.5 for all PF-PC synaptic connections. The weight change is given by

$$w_{i,j} = w_s + \Delta w_{i,j}, \tag{2}$$

where w_s is static component of the weight, the weight $w_{i,j}$ and $\Delta w_{i,j}$ depict the synaptic strength for input i, at PC j, and the change of weight accordingly.

The change of weight is the combination of the contribution of both LTP and LTD, as shown below.

$$\Delta w_{i,j} = w_{LTP} + w_{LTD} \tag{3}$$

Each one of these values is determined independently during the simulation.

The differential equation of w_{LTP} and w_{LTD} are respectively described by

$$\frac{dw_{LTP}}{dt} = \frac{-w_{LTP}}{\tau} \tag{4}$$

$$\frac{dw_{LTD}}{dt} = \frac{-w_{LTD}}{\tau} \tag{5}$$

in which τ is an variable shared decay term. These differential equations describe an exponential decay function towards zero, with a rate determined by the value of τ. The variable τ is a shared variable. It is created to capture the interaction between w_{LTP} and w_{LTD}. Without this term, both values, w_{LTP} and w_{LTD}, would eventually grow to their maximal value and the net change of weight would go to zero over time. There would be no long-lasting plasticity changes and all weights return to their original static value w_s. Therefore, the variable ensures that requirement *r2* is being met. Below, the equations for this parameter are described.

1) Decay term τ: The value of the decay term τ is determined at every time step of the simulation by

$$\tau(\tau_{max}, \eta, \sigma) = \tau_{max} \cdot \eta(w_{frac}, \alpha, \sigma_s, \kappa) \cdot \sigma(k, \Delta_{max}, w_{i,j}), \tag{6}$$

where the shared-decay parameters η and σ are defined by

$$\eta(w_{frac}, \alpha, \sigma_s, \kappa) = -\alpha \cdot e^{-0.5 \cdot (\frac{\frac{w_{frac}-0.5}{\sigma_s})^2}{\sigma_s \cdot \sqrt{2 \cdot \pi}})} + \kappa \tag{7}$$

$$\sigma(k, \Delta_{max}, w_{i,j}) = 1 - \frac{1}{1 + e^{-k \cdot (w_{LTP} + |w_{LTD}| - \Delta_{max} \cdot w_{i,j})}}. \tag{8}$$

In turn, w_{frac} is described by

$$w_{frac} = \frac{w_{LTP}}{w_{LTP} + |w_{LTD}|}. \tag{9}$$

In Appendix B all the different parameters of the decay term are presented. Each term captures an underlying biological observation, and is mathematically represented.

TABLE I
PHYSIOLOGICAL ACCURACY *p3* : SUB-PREREQUISITES

Prerequisites	**Elaboration**	**Validation**
Modulation	The present synaptic connections in the model need to modulate the postsynaptic activity. An example: PCs have an inhibitory connection to DCN. When PCs have a sudden increase in firing rate, one would expect to see an effect in the DCN (i.e. a decrease in firing rate)	Look at the raster plot of the network. Raster plots are used to study the neural responses by marking the events of spikes. It can also be used to see whether there is modulation at every synaptic connection.
Connectivity	The network has to be connected in a way that is congruent with anatomical observations.	The synaptic connections are based on anatomical observations, as found in literature. The connections are initially randomized where needed (e.g. 1 PC connects to 10 DCN), which are then set constant to compare different simulations.
Biological Plausibility	There are numerous assumptions made in modelling. The objective is to maintain the most important properties of the model and simplify where possible, while maintaining physiological and biological plausibility.	Bound certain cell properties to be within a viable range and evaluate firing frequencies.

2) Synaptic weight change Δw_{LTP} and Δw_{LTD}: It is assumed that LTP and LTD are directly linked to PC and IO cell spikes, respectively. The weight change that a spike brings about is evaluated using

$$\Delta w_k = w_{max,k} \cdot I_{d,k} \cdot f_{d,k} \cdot \rho_{d,k}, \tag{10}$$

in which the subscript k is either LTP or LTD, w_{max} is the maximal weight change, I_d is the input dependency, f_d is the frequency dependency, and ρ_d is the density dependency. The different dependencies of the synaptic weight changes are defined by

$$w_{max,k} = \frac{w_s \cdot \Delta_{max}}{t_{learn} \cdot f_k} \tag{11}$$

$$I_{d,k} = \frac{I_{tspike}}{I_{max}}, \tag{12}$$

$$f_{d,k} = \begin{cases} \frac{1}{1+e^{-k\cdot(f_{st}-\alpha f_{lt})}}, & \text{if } f_{st} \geq f_{lt} \\ 0, & \text{otherwise,} \end{cases}$$

$$\rho_{d,LTP} = 1 - \frac{1}{1+e^{-k\cdot(w_{LTP}-\alpha\cdot w_s\cdot\Delta_{max})}}, \tag{13}$$

$$\rho_{d,LTD} = \frac{1}{1+e^{-k\cdot(w_{LTD}-\alpha\cdot w_s\cdot\Delta_{max})}}. \tag{14}$$

All different terms of the equations are discussed in more detail in Appendix C.

III. RESULTS

The results consist of neuronal spiking behavior of the different cell types. By observing the population activity one can conclude whether the prior prerequisites are met and see emergent properties of the circuit. The synaptic weight change at PF-PC is analyzed as a function of PF input frequency. Subsequently, a dissection of the plasticity mechanism of two contrasting results is presented, which gives insight causation of the differences.

A. Neuronal Behavior

Figure 2 A shows a schematic representation of the model used in the experiments. It shows the different layers of cell types and visualizes the connectivity. The model consists of 10 PCs, 20 DCN and 20 IO cells. The size is chosen to represent a cerebellar module while remaining computationally tractable.
In Figure 2 B one can observe the raster plot of the network, which results from a sinusoidal PF input with an amplitude of 0.2 nA and a frequency of 10 Hz. Raster plots visualize the spike times of the different cells in the work. The following observations are made, based on the raster plot:

- Modulation at every level. IO spike causes pause in SS activity and consequently an increase in DCN activity, see yellow stripe.
- The input entrains the PC activity.
- DCN have an increase in firing rate if the PC pauses.
- The firing rate of the DCN shows peak activity with a rhythmicity around the same frequency as the input, as depicted by the red stripe.
- The population frequency of the IO shows a high level of synchrony, see green stripe.
- As for the DCN, the IO population activity shows consistent peaks around 10 Hz.

In Figure 2 C all the weight changes for all PCs are shown over a period of 14 seconds. The input that results in this weight changes is a sinusoidal wave form with a frequency of 15 Hz and an amplitude of 0.2 nA. The plasticity mechanism starts operating at six seconds, since the delta weight starts changing at that time. It can be seen that the weights follow different trajectories and settle on different values, as *r2* demanded. It can also be seen that the weights do not grow without bounds and it can be concluded that PCs are able to balance the two plasticity mechanisms.
Figure 2 D shows the final weights after the simulation of 20 seconds, of which the last 14 seconds the plasticity mechanism at PF-PC synapse is active. The first six seconds are not evaluated since cells showed transient behavior.

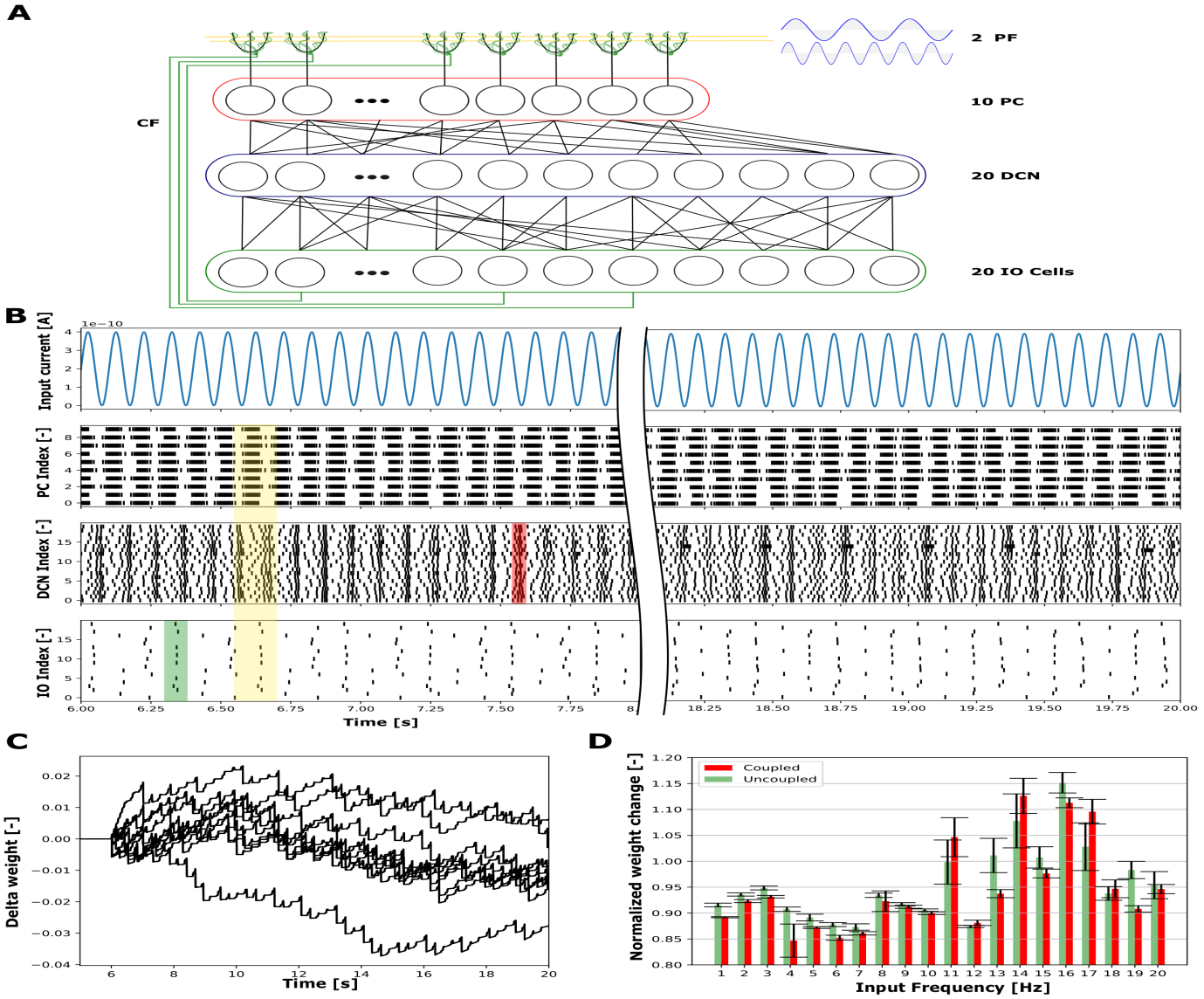

Fig. 2. Overview of results of modelling. **A** : Schematic representation of the olivocerebellar system. The inputs from the parallel fiber (PF) are generated by the user. PCs are connected, with a 1:10 ratio, to deep cerebellar nuclei (DCN), which are connected with a 1:10 ratio to inferior olive (IO) cells. 10 randomly selected IO cells are connected with 1:1 ratio to PCs via climbing fibers (CF). **B** : Raster plot together with input. The input from PF is here set to 10 Hz with an amplitude of 0.2 nA. The spike times of PCs, DCN, and IO cells are visualized in the raster plot. The time scale of the x-axis is chosen, to capture certain properties of the circuit. The modulation from the input to the PC is clearly visible, i.e. the input entrains the firing time of the PC. **C** : Weight change of all PC-PF weights. The change of weights over time is represented here with the new plasticity rule. The plasticity occurs for a time frame of fourteen seconds. **D** : Overview of all normalized weight changes. The mean with an error bar of a single standard deviation is presented for frequencies from one to 20 Hz. PCs select certain frequency input by alteration of weight change and it may be said that it can filter these inputs over time.

As mentioned in Sec II, the IO cells can be coupled via gap junctions and the synaptic weight change is evaluated with and without this property. The property does not show distinct differences in weight changes and is therefore, in this research, not further evaluated. Interestingly, this figure shows an emerging signal processing property of the PC. The PC shows a preference for certain PF input frequencies, as can be concluded from the observation that certain input frequencies result in LTD and others in LTP. In accordance with this observation, it is worth noting that the distinction between frequencies mainly occurs at the higher end of the frequency spectrum. Neighbouring frequencies show a sharp contrast in weight change. This feature is most distinct between 15 and 16 Hz. Since the simulations are recorded and all data can be analyzed, one can answer the question why this is the case.

B. Comparing weight change 15 and 16 Hz with coupled IO cells

The contrast between the final weight of 15 and 16 Hz is quite significant. The dissection of the plasticity mechanism is shown in Figure 3. The PF input of 15 Hz

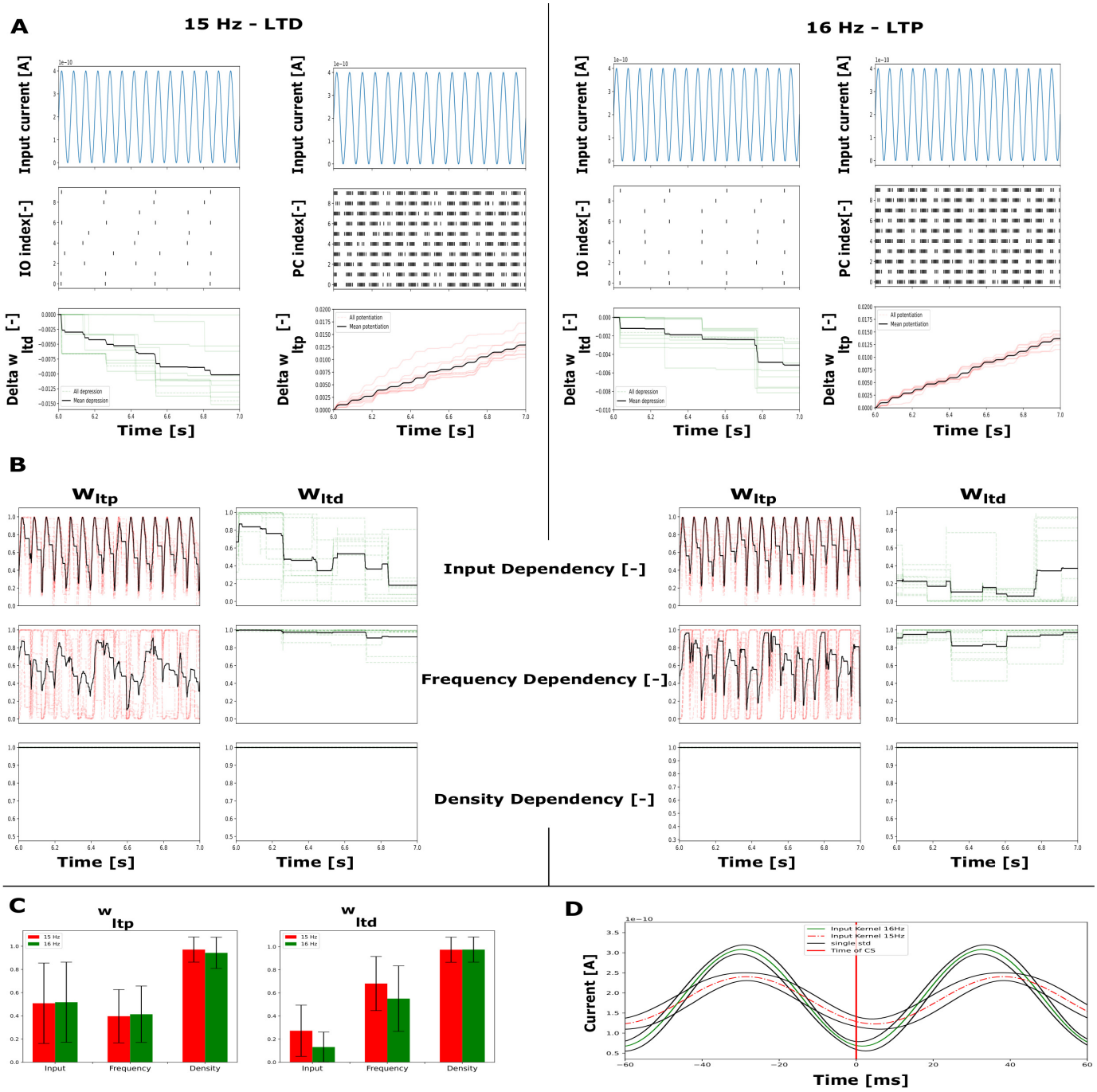

Fig. 3. Dissection of the plasticity mechanism. **A** : The comparison between 15 and 16 Hz PF input frequency is presented and their corresponding weight changes. **B** : Separation of all dependencies for Δw_{LTP} and Δw_{LTD} for a single second time frame. The input dependence for w_{LTD} is smaller for 16 Hz as for 15 Hz. Other values are similar. **C** : Averages over the entire simulation of the different dependencies with a single standard deviation. For potentiation the dependencies are similar. The mean for the input dependence of depression differ in their mean value (σ_{15Hz} = 0.272, σ_{16Hz} = 0.131) and are therefore the major reason for potentiation. **D** : PF input kernel before CS. At the time of the CS, the input for 16 Hz is smaller than for 15 Hz. The amplitude of the sinusoidal shape kernel is larger for 16 Hz. And there is a phase shift between the two signals.

leads to LTD while 16 Hz leads to LTP. By taking a look at the dependencies of the plasticity mechanism for 15 and 16 Hz, the causation for this contrast can be found. As described in Section II-C, the amount of weight change has three dependencies which are evaluated at the time of the spike. The PF input is shown in the top plot in Figure 3 A. The time window is set to a single second since it makes the effect of the spikes the clearest. IO cells that synapse onto PCs and therefore contribute to w_{LTD} are presented in the plot below. Since there are ten PCs, there are also ten IO cells shown in the raster, even though the network consists of 20 IO cells. PC spike times, and the corresponding Δw_{LTP} are presented for both frequencies.

The amount of w_{LTP} is on average similar for 15 and 16 Hz, but there is a higher variance for 15 Hz. The average of w_{LTD} is smaller for 16 Hz compared to 15 Hz, even tough there are some IO cells that do not depress at all. Therefore, it can be suggested the reason why 16 Hz causes LTP while 15 Hz causes LTD, has to be sought in the difference of w_{LTD}.
In Figure 3 B, all the dependencies are presented for both w_{LTP} and w_{LTD}. By simply looking at the different dependencies for the input and comparing the different frequencies, one can observe that w_{LTP} is similar, while w_{LTD} is larger for 15 Hz as compared to w_{LTD} of 16 Hz. The frequency dependency shows no clear difference between the two frequencies. The last dependency shows the density dependency, which is equal to one in both cases. This is expected since it represents the proximity of the w_{LTP} and w_{LTD} to its maximal value, and the time window is taken in the beginning of the simulation, so both values are nowhere near their maximum.
The mean of the dependencies over the entire simulation are visualized in Figure 3 C. In the left plot of w_{LTP}, it can be seen that the dependencies for w_{LTP} show no significant differences. The dependencies on the figure on the right confirm the previous observation that the input dependency of w_{LTD} is lower for 16 Hz than for 15 Hz.

Thus, the input at the time of the IO spike is lower for 15 Hz than for 16 Hz which, respectively leads to a depression and potentiation of PF-PC synapse. In Figure 3 D, the kernel of PF input at the time of the CS is presented. The kernel is obtained by averaging the PF input, before the IO produces a CS, over all PCs and all related CSs. Congruent with previous observations, the kernel of 16 Hz shows a lower current at the time of CS, compared to the kernel of 15 Hz. Both kernels show a sinusoidal shape with its minima close to the CS. While the minima are close together, there is still a phase shift visible. The amplitude of the 16 Hz kernel is significantly larger than the 15 Hz kernel.

IV. Discussion

A. Prerequisites of the Model

There are three prerequisites of the model presented in Sec I. Physiological accuracy *p3* was divided into three sub-prerequisites, as given by Table I. Whether the model meets the prerequisites can be concluded from the results.

Prerequisite *p1* states that our model should show functionality in the context of learning. Our model shows a novel signal processing property of the PC, which can be placed in the context of learning.
Prerequisite *p2* is met because the plasticity mechanism is based on physiological properties of the loop, which causes the synaptic weight change to adapt in an unsupervised manner.

The first of the three sub-prerequisites of *p3* states that there should be modulation at every synaptic connection. In the yellow transparent stroke of Figure 2 B, one can observe that there is modulation at every level. In other words: the PCs modulate the DCN activity, the DCN affect the IO cells, and the IO cells cause a CS in the PC. This is tuned by altering the amount of postsynaptic current based on the event of a presynaptic spike. Setting the postsynaptic current too high resulted in a complete silencing of the postsynaptic cell (in the case of an inhibitory connection), while setting the value too low resulted in no alteration of the postsynaptic membrane potential.
The second sub-prerequisite of *p3* states that the connectivity should be in line with anatomical observations. This is done by creating random connectivity with the proper ratio of synaptic connections. This randomization of connectivity was done once, and the resulting connectivity was used for further simulations, since it enables the possibility to preform analysis across different frequency inputs and to compare the results. The connectivity of the loop is the same across the different simulations.
The final sub-prerequisite of *p3* states that our model has to be biologically plausible. The arbitrary choice was made to evaluate the firing rates of the different cells. The firing rates of the different cells are within a plausible range: PC $\sim$ 100 Hz, DCN $\sim$ 30 Hz [46], and IO cell $\sim$ 1 Hz. While there are always improvements to be made in terms of modelling, we felt confident to take a leap of faith and analyse the emergent properties, drawn from reverse-engineering.

B. Requirements of the Plasticity Mechanism

The requirements of the long-term plasticity mechanism, mentioned in Sec I, are discussed. The first requirement *r1* states that it should be able to account for different firing frequencies of PC and IO, since PC spikes are assumed to be linked to LTP and spikes of the IO cell to LTD. While these firing frequencies differ significantly, $\sim$ 100 and $\sim$ 1 Hz for PC and IO respectively, it is accounted for by including a moving average of the two types of cells in question and making the maximum amount of weight change that a spike brings about dependent on that firing frequency. The relative weight change is therefore dependent on the firing rate of the cells and the long-term plasticity can account for those changes.
The second requirement *r2* declares that the weights of the different cells should not settle at the same level. If this would be the case, then there would be no selectivity of inputs by the PC. In Figure 2 C, it can be seen that, during the adaptation of the weights, the weights do not settle at the same level. The requirement is met due to the decay-term τ. Without this term, both w_{LTP} and w_{LTD} would reach their maximal value and a resulting net weight change of zero.

The third requirement *r3* states that the weight change should only occur if the change in firing rate is causally linked to presynaptic activity. Since PCs also spike spontaneously and are therefore not necessarily related to presynaptic activity. The most direct term that ensures this

property is the frequency dependency of the plasticity mechanism, as described in Section II-C. By comparing the short- and long-term frequency of the postsynaptic cell, one can quantify the extend to which the spike is linked to presynaptic activity.
The fourth requirement *r4* states that the weight should not grow without bounds. Both w_{LTP} and w_{LTD} are bounded by a maximal value. This is done by evaluating the current value at the time of the spike and comparing it to the maximal value via a sigmoidal function. In other words, the contribution of the weight change at the time of the spike, is dependent on the distance to its maximal value. If the current value is close to its minimum, the value does not hinder the weight change. When it is close to its maximum, the weight change is brought to a stop. The shape of this function that evaluates this parameter is sigmoidal. The sigmoidal shape is chosen since it is commonly used to describe other biological phenomena, such as mechanical muscle properties [47], and activation functions of neurons [48].
The final requirement *r5* has common ground with the previous one. Homeostasis should be ensured, i.e. stability during the ongoing process, at the synaptic level and for the entire network. In the case that there is no input, homeostasis in obviously present due to the input dependency. When there is no input, the dependency will be zero and there will be no weight changes. When the weight changes over time, it is bounded by the previously mentioned condition. When there is no plasticity at play during the simulation, the level of decay towards the original, static value is dependent on the original value of τ_{max}, as described in Table III.

C. Discussion of Emergent Properties

The aforementioned requirements and prerequisites are arbitrary and in complete control of the user of the model. Not all aspects of the olivocerebellar system can be modelled with the same physiological accuracy. The model does not have any inhibitory interneurons which are present on the molecular layer. These types of neurons modulate the response of the granule cell to produce better activity patterns [49]. While these cells shape the PF input, it does not alter the dynamics of the olivocerebellar loop. So within the prerequisites of the model in this research, the analysis has merit and can be possibly linked to physiological observations and high-level functioning.

In Figure 2 D, it can be seen that most PF-PC synapse undergo LTD. While it was long thought that LTD plays a predominant role in motor learning, it was recently shown that it is not essential [50]. Together with the finding that LTP prominently contributes to cerebellar motor learning [51], it may be suggested, that the presented finding suggest a selection of frequency input required for motor learning at the PC synapse.
Since the presented data of plasticity dependencies is for a single network with a single randomization of cell parameters, there is merit in running the simulation with new cell randomization and observe the synaptic weight changes. The synaptic weight change can then be linked to certain cellular properties, such as leak conductance or the adaptation time constant. Furthermore, the observed selection of frequencies can be validated in a statistical manner by running the simulation multiple times and adding noise (e.g. white Gaussian) to the sinusoidal PF input.

It can observed in Figure 3 C, that between 15 and 16 Hz, the driving difference of LTP and LTD comes from the input dependency of w_{LTD}. This suggests that potentiation of the synapse does not come from PF stimulation but is governed by the temporal spiking property of the IO cell.

The next steps in gaining a better understanding of the functioning of the cerebellar system would be to place the model in context of motor commands and actual feedback coming from a dynamical system. Such a dynamical system could be a robotic arm, that learns by means of motor babbling, which is a strategy infants use by moving their limbs without a specific goal. The only 'goal' is get familiar with their own dynamics and kinematics. The cellular behavior can then be observed with more 'realistic' input to the system.

V. Conclusions

This thesis proposed an olivocerebellar model with a focus on the balancing of long-term plasticity at the level of the PC. The prior requirements, based on biological constraints, were met for both the phenomenological model, as for the plasticity mechanism.
It was shown that the PC is able to balance the two forms of plasticity in context of sinusoidal PF input. The analysis of ranging the frequency input showed that, while most low frequency input led to depression of the weights, there is a highly non-linear weight change for high frequency inputs. The PC can distinguish different frequencies and may select certain aspect of the PF input signal which is relevant for motor learning.

References

[1] H. Ackermann, M. Vogel, D. Petersen, and M. Poremba, "Speech deficits in ischaemic cerebellar lesions," *Journal of neurology*, vol. 239, no. 4, pp. 223–227, 1992.

[2] B. Baier, P. Stoeter, and M. Dieterich, "Anatomical correlates of ocular motor deficits in cerebellar lesions," *Brain*, vol. 132, no. 8, pp. 2114–2124, 2009.

[3] I. Daum, M. M. Schugens, H. Ackermann, W. Lutzenberger, J. Dichgans, and N. Birbaumer, "Classical conditioning after cerebellar lesions in humans." *Behavioral neuroscience*, vol. 107, no. 5, p. 748, 1993.

[4] B. P. van de Warrenburg, J. A. Steijns, M. Munneke, B. P. Kremer, and B. R. Bloem, "Falls in degenerative cerebellar ataxias," *Movement disorders*, vol. 20, no. 4, pp. 497–500, 2005.

[5] R. Llinas and M. N. Negrello, "Cerebellum," *Scholarpedia*, vol. 10, no. 1, p. 4606, 2015.

[6] E. J. Lang, R. Apps, F. Bengtsson, N. L. Cerminara, C. I. De Zeeuw, T. J. Ebner, D. H. Heck, D. Jaeger, H. Jörntell, M. Kawato *et al.*, "The roles of the olivocerebellar pathway in motor learning and motor control. a consensus paper," *The Cerebellum*, vol. 16, no. 1, pp. 230–252, 2017.

[7] J. S. Albus, "A theory of cerebellar function," *Mathematical biosciences*, vol. 10, no. 1-2, pp. 25–61, 1971.

[8] W. T. Thach, H. Goodkin, and J. Keating, "The cerebellum and the adaptive coordination of movement," *Annual review of neuroscience*, vol. 15, no. 1, pp. 403–442, 1992.

[9] S. G. Lisberger, "The neural basis for learning of simple motor skills," *Science*, vol. 242, no. 4879, pp. 728–735, 1988.

[10] J. J. Kim and R. E. Thompson, "Cerebellar circuits and synaptic mechanisms involved in classical eyeblink conditioning," *Trends in neurosciences*, vol. 20, no. 4, pp. 177–181, 1997.

[11] Z. Gao, B. J. Van Beugen, and C. I. De Zeeuw, "Distributed synergistic plasticity and cerebellar learning," *Nature Reviews Neuroscience*, vol. 13, no. 9, pp. 619–635, 2012.

[12] S. G. Lisberger, "Internal models of eye movement in the floccular complex of the monkey cerebellum," *Neuroscience*, vol. 162, no. 3, pp. 763–776, 2009.

[13] W. Kakegawa, A. Katoh, S. Narumi, E. Miura, J. Motohashi, A. Takahashi, K. Kohda, Y. Fukazawa, M. Yuzaki, and S. Matsuda, "Optogenetic control of synaptic ampa receptor endocytosis reveals roles of ltd in motor learning," *Neuron*, vol. 99, no. 5, pp. 985–998, 2018.

[14] F. Crepel and J. Mariani, "Multiple innervation of purkinje cells by climbing fibers in the cerebellum of the weaver mutant mouse," *Journal of neurobiology*, vol. 7, no. 6, pp. 579–582, 1976.

[15] A. M. Lohof, N. Delhaye-Bouchard, and J. Mariani, "Synapse elimination in the central nervous system: functional significance and cellular mechanisms," *Reviews in the neurosciences*, vol. 7, no. 2, pp. 85–102, 1996.

[16] P. Strata and F. Rossi, "Plasticity of the olivocerebellar pathway," *Trends in neurosciences*, vol. 21, no. 9, pp. 407–413, 1998.

[17] C. Hansel and D. J. Linden, "Long-term depression of the cerebellar climbing fiber-Purkinje neuron synapse," *Neuron*, vol. 26, no. 2, pp. 473–482, 2000.

[18] M. Coesmans, J. T. Weber, C. I. De Zeeuw, and C. Hansel, "Bidirectional parallel fiber plasticity in the cerebellum under climbing fiber control," *Neuron*, vol. 44, no. 4, pp. 691–700, 2004.

[19] E. Lang, I. Sugihara, and R. Llinás, "Gabaergic modulation of complex spike activity by the cerebellar nucleoolivary pathway in rat," *Journal of Neurophysiology*, vol. 76, no. 1, pp. 255–275, 1996.

[20] R. Llinás and K. Sasaki, "The functional organization of the olivocerebellar system as examined by multiple purkinje cell recordings," *European Journal of Neuroscience*, vol. 1, no. 6, pp. 587–602, 1989.

[21] T. A. Blenkinsop and E. J. Lang, "Block of inferior olive gap junctional coupling decreases purkinje cell complex spike synchrony and rhythmicity," *Journal of Neuroscience*, vol. 26, no. 6, pp. 1739–1748, 2006.

[22] I. Lampl and Y. Yarom, "Subthreshold oscillations and resonant behavior: two manifestations of the same mechanism," *Neuroscience*, vol. 78, no. 2, pp. 325–341, 1997.

[23] Y. Manor, Y. Yarom, E. Chorev, and A. Devor, "To beat or not to beat: a decision taken at the network level," *Journal of Physiology-Paris*, vol. 94, no. 5-6, pp. 375–390, 2000.

[24] D. Armstrong, B. Cogdell, and R. Harvey, "Discharge patterns of purkinje cells in cats anaesthetized with alpha-chloralose." *The Journal of Physiology*, vol. 291, no. 1, pp. 351–366, 1979.

[25] R. Llinás and M. Mühlethaler, "Electrophysiology of guinea-pig cerebellar nuclear cells in the in vitro brain stem-cerebellar preparation." *The Journal of Physiology*, vol. 404, no. 1, pp. 241–258, 1988.

[26] C. I. De Zeeuw, C. C. Hoogenraad, S. Koekkoek, T. J. Ruigrok, N. Galjart, and J. I. Simpson, "Microcircuitry and function of the inferior olive," *Trends in neurosciences*, vol. 21, no. 9, pp. 391–400, 1998.

[27] L. N. Cooper and M. F. Bear, "The bcm theory of synapse modification at 30: interaction of theory with experiment," *Nature Reviews Neuroscience*, vol. 13, no. 11, pp. 798–810, 2012.

[28] L. Cooper, B. Lundquist, and S. Lundquist, "Proceedings of the nobel symposium on collective properties of physical systems," 1973.

[29] S. Diwakar, J. Magistretti, M. Goldfarb, G. Naldi, and E. D'Angelo, "Axonal na+ channels ensure fast spike activation and back-propagation in cerebellar granule cells," *Journal of neurophysiology*, vol. 101, no. 2, pp. 519–532, 2009.

[30] L. N. Cooper, F. Liberman, and E. Oja, "A theory for the acquisition and loss of neuron specificity in visual cortex," *Biological cybernetics*, vol. 33, no. 1, pp. 9–28, 1979.

[31] E. L. Bienenstock, L. N. Cooper, and P. W. Munro, "Theory for the development of neuron selectivity: orientation specificity and binocular interaction in visual cortex," *Journal of Neuroscience*, vol. 2, no. 1, pp. 32–48, 1982.

[32] C. Von der Malsburg, "Self-organization of orientation sensitive cells in the striate cortex," *Kybernetik*, vol. 14, no. 2, pp. 85–100, 1973.

[33] M. M. Nass and L. N. Cooper, "A theory for the development of feature detecting cells in visual cortex," *Biological cybernetics*, vol. 19, no. 1, pp. 1–18, 1975.

[34] D. O. Hebb, *The organization of behavior: a neuropsychological theory*. J. Wiley; Chapman & Hall, 1949.

[35] A. Geminiani, A. Pedrocchi, E. DâAngelo, and C. Casellato, "Response dynamics in an olivocerebellar spiking neural network with nonlinear neuron properties," *Frontiers in computational neuroscience*, vol. 13, p. 68, 2019.

[36] C. Casellato, A. Antonietti, J. A. Garrido, R. R. Carrillo, N. R. Luque, E. Ros, A. Pedrocchi, and E. D'Angelo, "Adaptive robotic control driven by a versatile spiking cerebellar network," *PLoS one*, vol. 9, no. 11, p. e112265, 2014.

[37] E. J. Lang, I. Sugihara, J. P. Welsh, and R. Llinás, "Patterns of spontaneous purkinje cell complex spike activity in the awake rat," *Journal of Neuroscience*, vol. 19, no. 7, pp. 2728–2739, 1999.

[38] M. Negrello, P. Warnaar, V. Romano, C. B. Owens, S. Lindeman, E. Iavarone, J. K. Spanke, L. W. Bosman, and C. I. De Zeeuw, "Quasiperiodic rhythms of the inferior olive," *PLoS computational biology*, vol. 15, no. 5, p. e1006475, 2019.

[39] R. Saegusa, G. Metta, G. Sandini, and S. Sakka, "Active motor babbling for sensorimotor learning," in *2008 IEEE International Conference on Robotics and Biomimetics*. IEEE, 2009, pp. 794–799.

[40] T. J. Ruigrok, "Ins and outs of cerebellar modules," *The cerebellum*, vol. 10, no. 3, pp. 464–474, 2011.

[41] R. Brette and W. Gerstner, "Adaptive exponential integrate-and-fire model as an effective description of neuronal activity," *Journal of neurophysiology*, vol. 94, no. 5, pp. 3637–3642, 2005.

[42] V. Steuber, N. W. Schultheiss, R. A. Silver, E. De Schutter, and D. Jaeger, "Determinants of synaptic integration and heterogeneity in rebound firing explored with data-driven models of deep cerebellar nucleus cells," *Journal of computational neuroscience*, vol. 30, no. 3, pp. 633–658, 2011.

[43] N. R. Luque, F. Naveros, R. R. Carrillo, E. Ros, and A. Arleo, "Spike burst-pause dynamics of purkinje cells regulate sensorimotor adaptation," *PLoS computational biology*, vol. 15, no. 3, p. e1006298, 2019.

[44] E. De Schutter and J. M. Bower, "An active membrane model of the cerebellar purkinje cell. i. simulation of current clamps in slice," *Journal of neurophysiology*, vol. 71, no. 1, pp. 375–400, 1994.

[45] N. Schweighofer, K. Doya, and M. Kawato, "Electrophysiological properties of inferior olive neurons: a compartmental model," *Journal of neurophysiology*, vol. 82, no. 2, pp. 804–817, 1999.

[46] S. Abbasi, A. Abbasi, Y. Sarbaz, and P. Shahabi, "Contribution of somatic and dendritic sk channels in the firing rate of deep cerebellar nuclei: Implication in cerebellar ataxia," *Basic and clinical neuroscience*, vol. 7, no. 1, p. 57, 2016.

[47] A. R. Gordon and M. J. Siegman, "Mechanical properties of smooth muscle. i. length-tension and force-velocity relations," *American Journal of Physiology-Legacy Content*, vol. 221, no. 5, pp. 1243–1249, 1971.

[48] A. C. Marreiros, J. Daunizeau, S. J. Kiebel, and K. J. Friston, "Population dynamics: variance and the sigmoid activation function," *Neuroimage*, vol. 42, no. 1, pp. 147–157, 2008.

[49] D. S. Touretzky, "MarrÂAlbus Model of Cerebellum Computational Models of Neural Systems Lecture 2.2," 2013.
[50] M. Schonewille, Z. Gao, H.-J. Boele, M. F. V. Veloz, W. E. Amerika, A. A. Šimek, M. T. De Jeu, J. P. Steinberg, K. Takamiya, F. E. Hoebeek *et al.*, "Reevaluating the role of ltd in cerebellar motor learning," *Neuron*, vol. 70, no. 1, pp. 43–50, 2011.
[51] M. Schonewille, A. Belmeguenai, S. Koekkoek, S. H. Houtman, H.-J. Boele, B. Van Beugen, Z. Gao, A. Badura, G. Ohtsuki, W. Amerika *et al.*, "Purkinje cell-specific knockout of the protein phosphatase pp2b impairs potentiation and cerebellar motor learning," *Neuron*, vol. 67, no. 4, pp. 618–628, 2010.

APPENDIX

A. Appendix A: Code description

A github repository is made to track the process of modelling of the olivocerebellar system. The modelling is done with use of *Brian2* in Jupyter notebooks and stand-alone *Python*-files. From here, one can pull the repository and reproduce the results presented in this paper. The github repository is the following:
https://github.com/ThijsHoedemakers/CerebellarLoop.git

Here a brief overview of the different files are presented that acts as a guide through the simulation process.

A Functions: Set up functions that are used throughout the rest of the code. The different functions are:

1) Visualise : visualise the connection between the different cell types.
2) rand params : randomize the cell parameters.
3) NoiseGenerator : Create the PF input.

B StartUp: The different cell parameters are either randomized when no run is done before, or the parameters from a prior simulation are used. The parameters will later be used for the construction of aEIF neurons (PCs and DCN) and the two-compartment model for the IO cells.

C Equations: The prior generated input signal of the *NoiseGenerator*-function is loaded in and simulated as a neuron group. This group will later be used to connect to a dummy neuron, which is connected to the PCs. The dummy neurons pass the input from the PF with a multiplication factor. This multiplication factor changes due to the implemented plasticity mechanism.
The differential equations of PCs and DCN are given based on [41]. Also, the adaptation of the Schweighofer [45] is presented here.
The equations that drive PF-PC synaptic weight change are given here. The difference between coupled and uncoupled is already made since it makes it easier to use later on. It consists of the dependencies, as described in Section II.

D NeuronGroups: From this file onward, a distinction has to be made between 'Plasticity' and 'NoPlasticity', since both simulation will be ran parallel. The file creates the cell groups for the coupled and uncoupled scenario and takes the randomized cell parameters to do that.
The cellular activity is monitored. There are different types of monitors of cell activity:

1) StateMonitor : tracks time evolution of cellular variables
2) PopulationRateMonitor : tracks firing rate of a population of cells
3) SpikeMonitor : tracks spikes of cells

All the required data is monitored during the simulation and later used for analysis.

E New Plasticity: The plasticity mechanisms use the long- and short-term averages of the firing rates to determine the effect a spike brings about. For the firing rate of the IO cells the interspike-interval (ISI) is taken and averaged, while for the PCs the moving average over a time window is taken. This has to do with the occurrence of the spikes. The pause in PC caused by the CS would not significantly influence the firing rate if one would look at the ISI, since it would only have a single value and its effect would be minimal. Therefore it would not accurately depict the firing rate of the PC.

E Synapses: The synapses between the different cell types are created here. A distinction is made between the fixed and randomized connectivity, since the simulation is only comparable if the connectivity remains constant. The connectivity for five and two PF inputs is already given.
The static weight of (2) is set to 0.5 for all synaptic connections. LTD and LTP are represented in the equations of the synaptic connections in event of a spike of the pre- or postsynaptic neuron.

F save data: All recorded data is stored in a *hfd5* structure, which uses groups and data-sets in a hierarchical structure. The data has the following structure:

- 1Hz
- 2Hz
  - Initial
    - Voltage Cells
    - Spikes
      - PC coupled/uncoupled
      - DCN coupled/uncoupled
      - IO cells coupled/uncoupled
    - Population rate
    - Input
    - Parameters Values
  - Plasticity
  - Adapted

  ⋮
- 20Hz

The data for the spikes of a 2Hz PF input, initial run,is now expanded. The same can be done for all frequencies, types of run, and recorded variables.

G plot: Visualize the different cell responses, extracted from the aforementioned monitors.

RunAll: To run multiple simulations consecutively, this file is created. It can be called from the command window with the following command:

```
for /l %i in (1,1,20) do for %k in (0,1,2)
do python RunAll.py 1 %i %k
```

in which i is the input frequency, and k represents the type of simulation (initial, plasticity, and adapted). With a simple adaptation to this command, one can put in a mixture of frequencies, which might be interesting for future research.

RunMe files: These files can be used to run a single simulation with or without plasticity. The advantage of using *RunAll.py* is that it can run multiple simulations after each other. When you only want a single run, the specified *RunMe* can be used.

Data Analysis pt2: The figures generated in this paper come from this *Jupyter*-notebook. For the first five seconds of the simulation no input is given to the system and is therefore removed from the data-set. The data that is used in the *.hfd5*-format exceeds the maximum size allowed on Github. If one would want to reproduce the results and figures, contact the author.

B. Appendix B: decay term

All parameters that make up the shared decay term τ are presented and discussed in Table III.

C. Appendix C : delta w

All the terms that make up the weight change are presented in the Table IV.

TABLE III
SHARED DECAY-TERM τ

Parameter		Description	Unit	Value
τ_{max}		The maximal value of the decay. The larger this value, the smaller the decay at every time step. It is also an indicator of how long the changes in weight maintain at their newly reached value.	[s]	800
$\eta(w_{frac}, \alpha, \sigma, \kappa)$ (Eq.(7))		Evaluates the value of w_{frac} at an inverse Gaussian with its center at 0.5 and its minimal value close to zero. It represents the level of competing between the two plasticity mechanisms. When both w_{LTP} and w_{LTD} are contributing to the total weight change, the shared decay term τ becomes smaller, which in turn makes the system remains receptive to the changes in both weights and the homeostasis between them.	[-]	~0 - 1
	w_{frac} (Eq.(9))	It evaluates the level of contribution of w_{LTP} to the total amount of weight change.	[-]	~0 - 1
	α	Constant that adjusts the size of the inverse Gaussian to range from zero to one.	[-]	0.0376
	σ_s	Standard deviation of the Gaussian function. The value determines the width of the Gaussian distribution. The higher this value, the less the level of competence has to be close to the center 0.5.	[-]	0.015
	κ	Constant that is used to move the inverse Gaussian vertically. This minimal value of the inverse Gaussian should be close to zero. However, it should not be exactly zero, since that would result in τ being zero, and a division by zero for the differential equation.	[-]	1.01
σ (Eq.(8))		Sigmoidal function that evaluates the total amount of weight change, i.e. the sum of w_{LTP} and w_{LTD}. The synaptic weight can change freely when the weight remains close to its original value. Once the weight reaches a value near its maximum, the value of σ descends, together with the decay. This way the dynamic relation between LTP and LTD is simulated.	[-]	~0 - 1
	k	Steepness of the sigmoidal function.	[-]	100
	Δ_{max}	Maximum amount of weight change in decimals.	[-]	0.1 - 0.4
	$w_{i,j}$	Current value of the weight	[-]	0-1

TABLE IV
ΔW

Parameter		Description	Unit	Value
$\Delta w_{LTP,LTD}$		The weight change of w_{LTP} and w_{LTD}. This value is added in the discrete event of a spike. The PC spike is responsible for the evaluation of Δw_{LTP} and the IO cell spike,that synapses onto the corresponding PC for Δw_{LTD}.	[-]	«1
	$w_{max,k}$	The maximal amount of synaptic change a weight can undergo in the event of a spike. It is dependent on the firing frequency and can therefore account for the inconsistent firing rate (*r1*).	[-]	«1
	w_s	The static component of the weight. The value is dependent on the amount of inputs and the amount of current coming from the inputs.	[-]	0.5
	Δ_{max}	Maximum amount of weight change.	[-]	0.1 - 0.4
	t_{learn}	A time scale constant which indicates at the time in which the maximum amount of potentiation or depression can be reached. A high value indicates that it takes a long time before the weights reach their maximum. This could be functionally linked to a learning a difficult task. For the sake of simulation it is set relatively low, to 'speed up' the results.	[s]	5
	f_k	Firing frequency of the cell: PC for LTP, IO for LTD.	[Hz]	1-10 - IO, 60-140 - PC
	$I_{d,k}$	The dependency of the input current at the moment of the spike. It shows the correlation between the input current and the produced spike	[-]	0 - 1
	I_{tspike}	The input current at the time of the spike.	[nA]	0 - 0.4
	I_{max}	The maximal value of the input current. This value is the result of tuning until the prior prerequisites are met (see Table I).	[nA]	0.4
	$f_{d,k}$	The frequency dependence compares the long-term firing rate and the short-term firing rate of the cell. The parameter $f_{d,k}$ is only larger than zero if the short-term firing rate is larger than the long-term firing rate. When this condition holds, the value increases in a graded manner, i.e. the larger the difference, the larger the value. The parameter captures the extend of influence the input has on the firing rate of the cell and the ascribed change in synaptic weight, as was prescribed by *r3*. Since both the parallel fiber and climbing fiber have an excitatory connections, the frequency dependence is solely based on the firing rate of the PC.	[-]	0-1
	k	Steepness of sigmoidal function	[-]	0.3
	f_{st}	Short-term firing rate of the cell. The value for the PC is based on the amount of spikes over a 150 ms interval, divided by 150 ms.	[Hz]	60-140 PC
	f_{lt}	Long-term firing rate of the cell. The value is derived in the same manner as the short-term firing rate, only the time window is now 5 s.	[Hz]	60-140 PC
	α	Constant to move the center of the sigmoidal function.	[-]	1.1
	$\rho_{d,k}$	Sigmoidal function that evaluates the current contribution of potentiation and depression. It represents the bounded amount of physiological properties that enable the potentiation and depression. If the potentiation or depression is close to its maximal value, the ρ parameter will approach zero, which means that without this parameter, w_{LTP} and w_{LTD} could grow without bounds, which is not biologically plausible. It ensures that requirement *r4* is met. The shape of the sigmoidal function differs due to the sign of w_{LTD}.	[-]	0 - 1
	k	Steepness of the sigmoidal function	[-]	200
	w_i	Current value of the w_{LTP} or w_{LTD}	[-]	0.4-0.6
	α	Constant to move the center of the sigmoidal function.	[-]	0.833
	w_s	The static component of the weight. The value is dependent on the amount of inputs and the amount of current coming from the inputs.	[-]	0.5
	Δ_{max}	Maximum amount of weight change	[-]	0.1 - 0.4